



Restoring p53 Function in Human Melanoma Cells by Inhibiting MDM2 and Cyclin B1/CDK1-Phosphorylated Nuclear iASPP

Min Lu, Hilde Breyssens, Victoria Salter, Shan Zhong, Ying Hu, Caroline Baer, Indrika Ratnayaka, Alex Sullivan, Nicholas R. Brown,⁶ Jane Endicott,⁶ Stefan Knapp,^{2,5} Benedikt M. Kessler,^{3,5} Mark R. Middleton,⁷ Christian Siebold,⁴ E. Yvonne Jones,⁴ Elena V. Sviderskaya,⁸ Jonathan Cebon,⁹ Thomas John,⁹ Otavia L. Caballero,¹⁰ Colin R. Goding,¹ and Xin Lu1,*

¹Ludwig Institute for Cancer Research

University of Oxford, Oxford OX3 7DQ, UK

SUMMARY

Nearly 90% of human melanomas contain inactivated wild-type p53, the underlying mechanisms for which are not fully understood. Here, we identify that cyclin B1/CDK1-phosphorylates iASPP, which leads to the inhibition of iASPP dimerization, promotion of iASPP monomer nuclear entry, and exposure of its p53 binding sites, leading to increased p53 inhibition. Nuclear iASPP is enriched in melanoma metastasis and associates with poor patient survival. Most wild-type p53-expressing melanoma cell lines coexpress high levels of phosphorylated nuclear iASPP, MDM2, and cyclin B1. Inhibition of MDM2 and iASPP phosphorylation with small molecules induced p53-dependent apoptosis and growth suppression. Concurrent p53 reactivation and BRAFV600E inhibition achieved additive suppression in vivo, presenting an alternative for melanoma therapy.

INTRODUCTION

Advanced melanoma often harbors activating mutations in the RAS-BRAF-MAPK, p16^{ink4a}-Rb, and p14^{ARF}-p53 tumor suppressor pathways. The importance of RAS and RAF oncogenes in melanoma development and maintenance is underscored by the recent success of BRAF inhibitors, such as vemurafenib, as therapeutic agents. Vemurafenib selectively inhibits the proliferation of tumor cells harboring the BRAFV600E mutation, which is present in \sim 50% of human melanomas (Joseph et al., 2010). Despite promising efficacy on initial treatment, most vemurafenib-treated patients relapse within months due to acquired drug resistance. Thus, cotargeting BRAFV600E and MEK has been suggested (Poulikakos and Solit, 2011).

An alternative would be to cotarget two independent pathways that are both critical in melanoma development and maintenance. The p53 tumor suppressor pathway is of particular interest. Over 80% of human melanomas express p53 that has the wild-type (WT) sequence but often has impaired function, some of which also have the BRAF water mutation. p53 inactivation can be achieved by a deletion in the $p16^{ink4a}$ locus, which inactivates both $p16^{ink4a}$ and $p14^{ARF}$, and occurs in \sim 50% of

Significance

Metastatic melanoma is resistant to treatment and accounts for 80% of skin cancer deaths. Restoring p53 function in melanoma is an attractive therapeutic strategy, as nearly 90% of human melanomas express functionally defective wildtype p53. Nutlin3, an agonist of p53, is currently in clinical trials, but often fails to reactivate p53 function when used alone. We found that concurrent inhibition of MDM2 and iASPP with small molecules resulted in p53-dependent apoptosis and growth suppression of melanoma cells in vitro and in vivo. Reactivation of p53 together with BRAFV600E inhibition induced apoptosis and suppressed melanoma growth, presenting an alternative strategy for melanoma therapy.



²Structural Genomics Consortium

³Centre of Cellular and Molecular Physiology

⁴Division of Structural Biology

⁵Target Discovery Institute, Nuffield Department of Clinical Medicine

⁶Department of Biochemistry, University of Oxford, South Parks Road, Oxford, OX1 3QU, UK

⁷Department of Oncology, Churchill Hospital, University of Oxford, Oxford OX3 7LE, UK

⁸Cell Signaling Research Centre, Division of Biomedical Sciences, St. George's, University of London, SW17 0RE, UK

⁹Ludwig Institute for Cancer Research, Austin Health, University of Melbourne, Victoria 3084, Australia

¹⁰Ludwig Collaborative Laboratory, Johns Hopkins University School of Medicine, MD 21231, USA

^{*}Correspondence: xin.lu@ludwig.ox.ac.uk http://dx.doi.org/10.1016/j.ccr.2013.03.013



melanomas (Curtin et al., 2005). Mutation of p14^{ARF} impairs its ability to prevent MDM2, an E3 ubiquitin ligase of p53, from targeting p53 for degradation (Zhang et al., 1998). The p53 stress signal response is often defective in p14^{ARF} mutant melanoma cells (Yang et al., 2005), and p53 prevents progression of nevi to melanoma in a transgenic mouse model (Terzian et al., 2010). Overexpression of MDM2 or MDMX, which bind and inactivate p53, is observed in melanomas (Gembarska et al., 2012; Muthusamy et al., 2006; Polsky et al., 2001).

To restore p53's tumor suppressive function in human tumors expressing WT p53, p53 agonists such as Nutlin3 have been developed (Vu and Vassilev, 2011). Nutlin3 suppresses tumor growth by preventing MDM2 from binding to and targeting p53 for degradation. However, Nutlin3 alone only causes modest reactivation of p53 in WT p53-expressing melanoma cells (de Lange et al., 2012; Ji et al., 2012) and induces only p53-mediated cell cycle arrest but not apoptosis (Tseng et al., 2010). Cell cycle arrest is a reversible process, whereas apoptosis is irreversible. Thus, the identification of ways to reactivate p53's apoptotic function is crucial. In over 60% of melanoma cell lines tested, WT p53 lost its normal transcriptional activities (Houben et al., 2011). p53-targeted apoptosis genes are often underexpressed in WT p53-expressing melanomas (Avery-Kiejda et al., 2011), thus WT p53 may lose its apoptotic function in these cells.

iASPP, which is encoded by PPP1R13L, is evolutionarily conserved from Caenorhabditis elegans to humans (Bergamaschi et al., 2003). The C termini of all three ankyrin repeat, SH3 domain, and proline-rich region containing protein (ASPP) members (ASPP1, ASPP2, and iASPP) have similar motifs and domain organization, but iASPP's N terminus is distinct from the others. Functionally, ASPP1 and ASPP2 stimulate, whereas iASPP inhibits, p53-induced apoptosis; mainly by preferentially regulating its transcriptional activity on apoptosis- (but not cell cycle arrest) related genes (Bergamaschi et al., 2006b; Samuels-Lev et al., 2001). Overexpression of iASPP is associated with chemoresistance in human cancer (Jiang et al., 2011). iASPP inhibits both cellular senescence in vitro and epithelial stratification of epidermis and esophagus in vivo. It is mostly expressed as a nuclear protein in basal epithelial cells that coexpress p63, typical of a proliferative epidermal compartment. iASPP becomes cytoplasmic in differentiated epithelial cells (Chikh et al., 2011; Notari et al., 2011). iASPP's N terminus is required for its cytoplasmic localization (Slee et al., 2004). Because many iASPP-interacting proteins are transcription factors (i.e., p53, p63, and NF-κB) (Bergamaschi et al., 2003; Notari et al., 2011; Yang et al., 1999), it is likely that nuclear iASPP is more active than cytoplasmic iASPP in regulating transcription. Thus, iASPP's ability to inhibit p53's apoptotic function in human melanoma was studied.

RESULTS

p53 Selectively Binds Slow-Migrating Nuclear iASPP that Is Enriched in Metastatic Melanomas

iASPP expression and localization in 142 human melanomas was examined. Cytoplasmic iASPP was mostly detected in primary melanomas, whereas nuclear iASPP was mainly found in metastases (Figure 1A). Most lymph node metastases expressed higher nuclear iASPP than primary tumors (>2-fold,

p < 0.05), suggesting an association with advanced stage cancers (Figure 1B). Full clinical follow-up information was available for 66/142 melanomas. High nuclear iASPP levels were associated with poor patient survival (Figure 1C, p < 0.01).

iASPP was mainly cytoplasmic in human primary melanocytes and in a panel of nonmelanoma tumor cell lines. However, nuclear iASPP was enriched in most of melanoma cell lines examined (Figure S1A available online; data not shown). Nuclear iASPP was detected in the WT p53-expressing melanoma cell line WM115 whereas both cytoplasmic and nuclear iASPP were detected in the mutant p53-expressing melanoma cell line SK-MEL37. Mainly, cytoplasmic iASPP was detected in the p53 null human lung cancer cell line H1299 (Figure 1D).

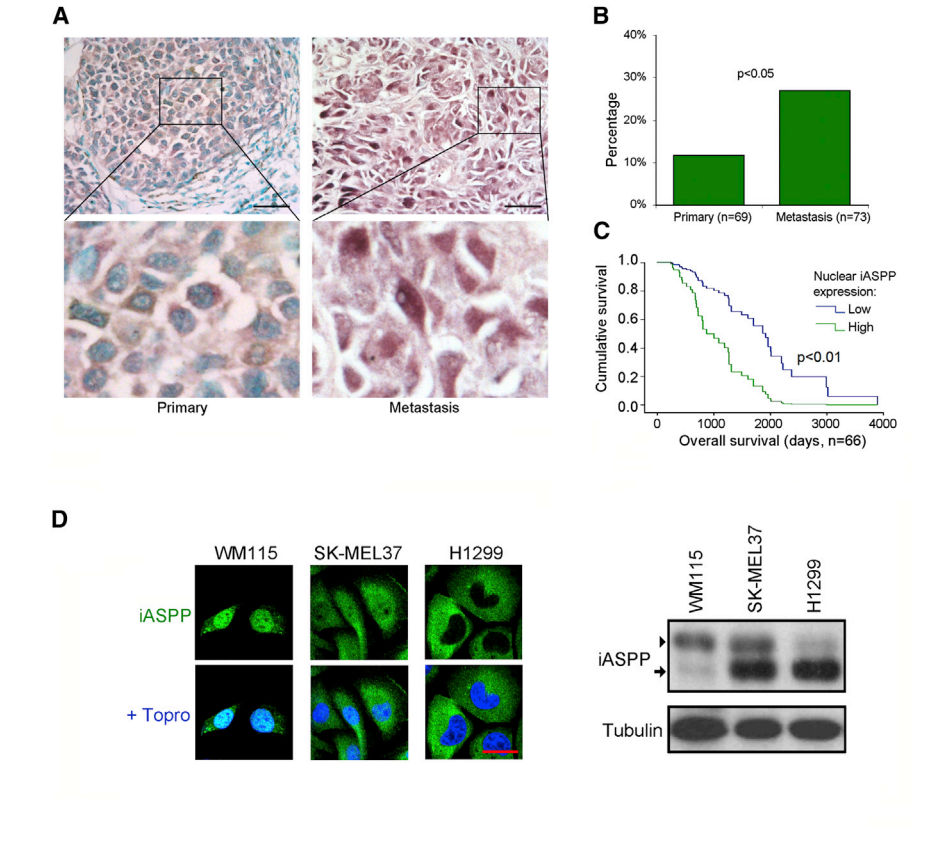
Although iASPP migrated as two bands in all three cell lines, it mostly migrated as a slower single band in WM115 but as a faster single band in H1299 cells. We detected two iASPP bands in SK-MEL37 cells, the mobilities of which corresponded with those detected in WM115 and H1299 cells (Figure 1D). Thus, nuclear localization of iASPP associates with slower migration. A similar association was seen in all cell lines examined (Figures S1B and S1C). p53 selectively coimmunoprecipitated slow-migrating iASPP in the panel of melanoma cell lines tested (Figure 1E). This was most evident in WM278 cells in which p53 mainly bound slow-migrating iASPP, even though its expression was lower than that of fast-migrating iASPP (Figure 1E). These data suggest that slow-migrating nuclear iASPP is a more active p53 inhibitor than fast-migrating cytoplasmic iASPP. This is consistent with the in vivo finding that nuclear iASPP is enriched in metastatic melanomas and associates with poor survival.

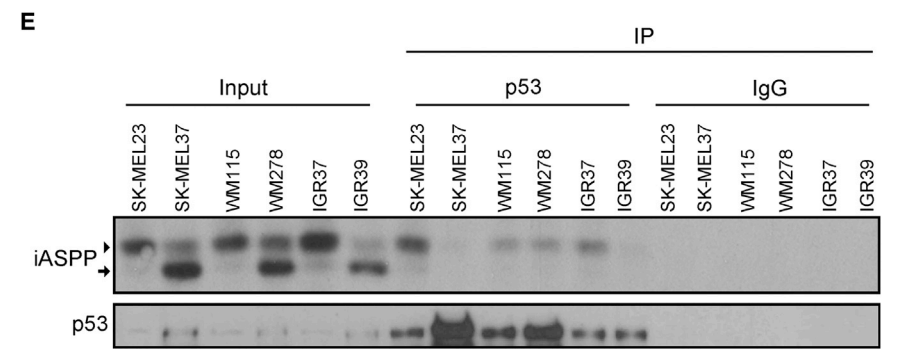
Mitotic Arrest Induces Slow-Migrating Nuclear iASPP

Treatment of H1299, WM278, and B16 cells with various agents showed that slow-migrating iASPP was specifically induced by mitotic inducers such as nocodazole, paclitaxel, and colchicine. Doxorubicin, staurosporine, cisplatin, and hydrogen peroxide, which do not induce mitosis, had minimal effect (Figure 2A). As mitotic cells often detach from tissue culture dishes, floating cells were separated from adherent cells after nocodazole and paclitaxel treatment. Figure 2B shows the enrichment of slowmigrating iASPP in floating cell populations of cells treated with mitotic inducers. Moreover, slow-migrating iASPP was mainly found in naturally occurring G2/M phase cells enriched by shake-off, confirmed by the presence of phosphohistone H3 (Figure 2C) and FACS analysis (Figure S2A). Nuclear iASPP was detected in some H1299 and most WM278 floating cells (Figure 2D). Adherent H1299 cells only expressed cytoplasmic iASPP whereas adherent WM278 cells expressed both forms (Figure 2C). Nocodazole clearly increased slow-migrating iASPP in a panel of melanoma lines expressing both slow and fastmigrating isoforms (Figure 2E), demonstrating that the observed regulation of iASPP migration is a general phenomenon.

H1299 and WM278 cells were treated with stimuli such as EDTA or cold shock to induce cell detachment but not mitosis. Both treatments failed to affect iASPP mobility in H1299 cells and had minimal effects on WM278, although nocodazole induced large increases in slow migrating iASPP under the same conditions (Figure S2B). These data show that mitotic signals induce slow-migrating iASPP, not cell detachment.







Phosphorylation of iASPP at S84/S113 by Cyclin B1/CDK1 Contributes to iASPP Slow Migration

To identify the iASPP regions responsible for slow migration, two V5-tagged iASPP truncation mutants, iASPP(1–478)-V5 and iASPP(482–828)-V5, were transfected into H1299 or SK-MEL37 cells, which mainly express unmodified iASPP. The transfected cells were treated with nocodazole or paclitaxel to induce mitosis. Mobility shifts were detected by anti-V5 antibody. Slow-migrating iASPP(1–478)-V5 was specifically induced in nocodazole or paclitaxel-treated cells (Figure 3A). Under the same conditions, iASPP(482–828)-V5 mainly migrated as a single band, indicating that modifications in the N-terminal half of iASPP are primarily responsible for slow migration of iASPP caused by mitotic inducers.

Recombinant N-terminal iASPP fragments iASPP(1-240) and iASPP(249-482) were tested in an in vitro kinase assay using

Figure 1. p53 Selectively Binds Slow-Migrating Nuclear iASPP that Is Enriched in Metastatic Melanomas

(A and B) Example of iASPP staining pattern (A) and the percentage of samples expressing high nuclear iASPP (B) in 142 human primary and metastatic melanoma tissue array cores. Scale bar represents $50~\mu m$.

(C) Survival curves of patients with low or high nuclear iASPP expression. n, number of samples analyzed.

(D) Immunofluorescence staining showing iASPP cellular localization (left panel, green) and immunoblot showing iASPP mobility (right panel) in indicated cells. Topro (blue) marks nuclei. Scale bar represents 20 µm.

(E) Immunoprecipitation to determine binding between endogenous iASPP and p53 in human melanoma cell lines as indicated. Cell lysates are labeled as input.

In (D) and (E), arrows and arrowheads mark positions of fast or slow-migrating iASPP isoforms respectively.

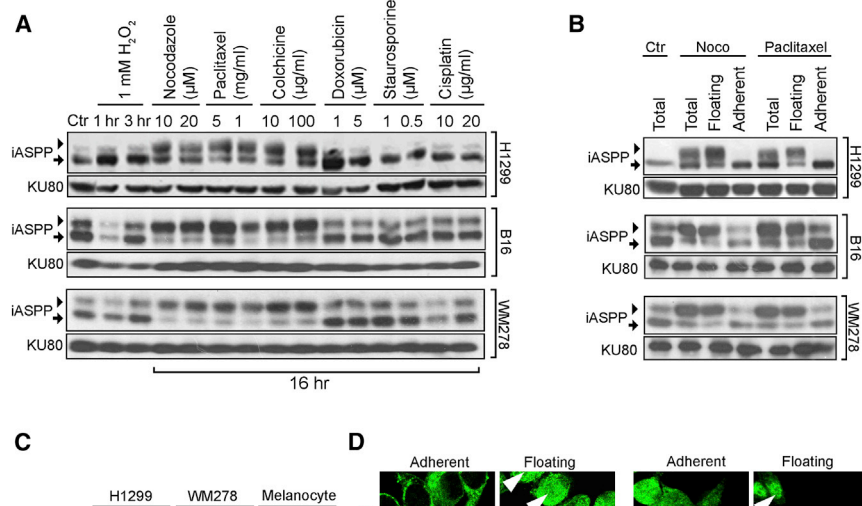
See also Figure S1.

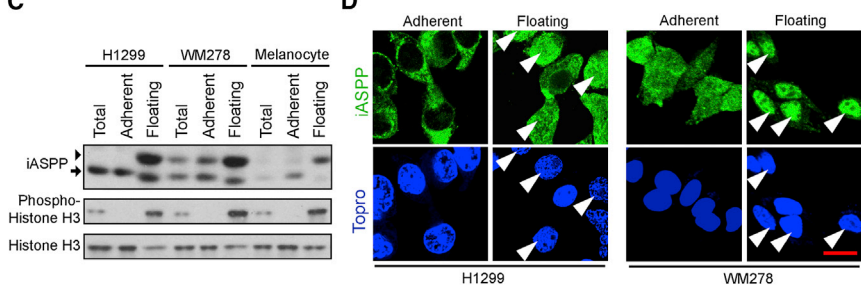
purified cyclin B1/CDK1. iASPP(1-240), but not iASPP(249-482), interacted with CDK1 and was phosphorylated by cyclin B1/CDK1 in vitro (Figures 3B and 3C). S84, S113, and S120 were identified as potential cyclin B1/CDK1 phosphorylation sites in iASPP(1-240). These sites were singly or doubly mutated to alanine to generate iASPP(1-240) mutants (S84A; S113A; S120A; S84A/S113A; S84A/S120A). The results in Figure 3D show that cyclin B1/CDK1 failed to phosiASPP(1-240)S84A/S113A, phorylate whereas all other phosphorylation mutants could be phosphorylated in vitro.

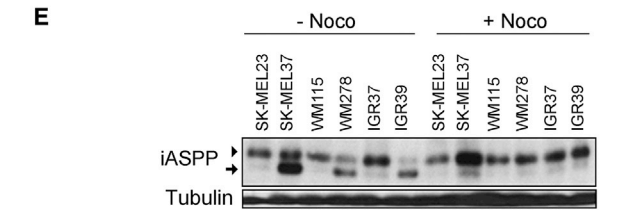
The impact of iASPP S84/S113 phosphorylation by cyclin B1/CDK1 on iASPP migration was tested by transfecting iASPP and its nonphosphorylatable and

phosphomimetic mutants, iASPP(S84A/S113A) and iASPP (S84D/S113D), into melanoma cell lines IGR37 and IGR39, which mainly express slow- and fast-migrating iASPP, respectively. In IGR37 and IGR39 cells, endogenous iASPP was mainly detected as slow and fast-migrating isoforms, respectively (Figure 3E, LX49.3 panel). Within the same set of lysates, slow-migrating iASPP-V5 was detected in IGR37 cells, whereas iASPP-V5 was fast-migrating in IGR39 cells. iASPP(S84D/S113D) produced partial slow-migrating iASPP in IGR37 cells, but not in IGR39 cells. In both IGR37 and IGR39 cells, iASPP(S84A/S113A) was as a single fast-migrating iASPP band (Figure 3E, iASPP-V5 panel). Thus, transfected iASPP-V5 has a similar migration pattern to endogenous iASPP. Phosphorylation of iASPP at S84 and S113 contributed to its slow migration in SDS-PAGE. Mass spectrometry analysis confirmed that endogenous iASPP from H1299 cells was phosphorylated on S84 and S113 in









nocodazole-treated cells, but not in untreated lysates (Figure S3; data not shown). Phosphoproteome analysis of HeLa cells also reported upregulation of S84 and S113 phosphorylation of iASPP during mitosis (Olsen et al., 2010). Thus, S84 and S113 are phosphorylated by cyclin B1/CDK1 both in vitro and in vivo, and their phosphorylation retards iASPP's migration.

S84/S113 Phosphorylation of iASPP Promotes iASPP **Nuclear Localization by Preventing N- and C-Terminal Self-Interaction**

Our previous structural study showed that iASPP's C-terminal p53 binding domain can be masked by a peptide (GSPRKARR) within iASPP (residues 615-622) (Robinson et al., 2008). This peptide shares high sequence similarity with the N-terminal region of iASPP, where S84 (GSPRKAAT) is located. Structural modeling predicted that iASPP's N-terminal domain may interact with its C terminus, and phosphorylation of iASPP at S84 may interfere with this (Figure S4A). Purified iASPP(1–240) but not iASPP(249-482) was found to interact with the purified iASPP C-terminal fragment, iASPP(625-828), which contains the ankyrin repeat and SH3 domains. Under the same conditions, iASPP(1-240) did not interact with the C terminus of ASPP2(905-1128), which has high sequence and structural

Figure 2. Mitotic Arrest Induces Slow-**Migrating Nuclear iASPP**

(A) iASPP is detected by immunoblotting in H1299. WM278, or B16 cells treated as indicated conditions (Ctr: DMSO).

(B) Various cells were treated with the indicated agents (Ctr, DMSO; Noco, nocodazole) for 16 hr. Floating and adherent cells were separated by cell shake-off. iASPP in cell lysates was immunoblotted.

(C) iASPP in floating and adherent H1299, WM278, or human primary melanocytes separated by cell shake-off was immunoblotted. Expression levels of total and phosphorylated histone H3 were used as a loading control and indicator of enrichment of G2/M cells, respectively.

(D) Collected floating cells were seeded onto slides by cytospin and stained with anti-iASPP antibody by immunofluorescence. White arrowheads point to nuclear iASPP. Scale bar represents 20 um.

(E) iASPP in human melanoma cell lines with or without 10 µM nocodazole treatment for 16 hr was immunoblotted.

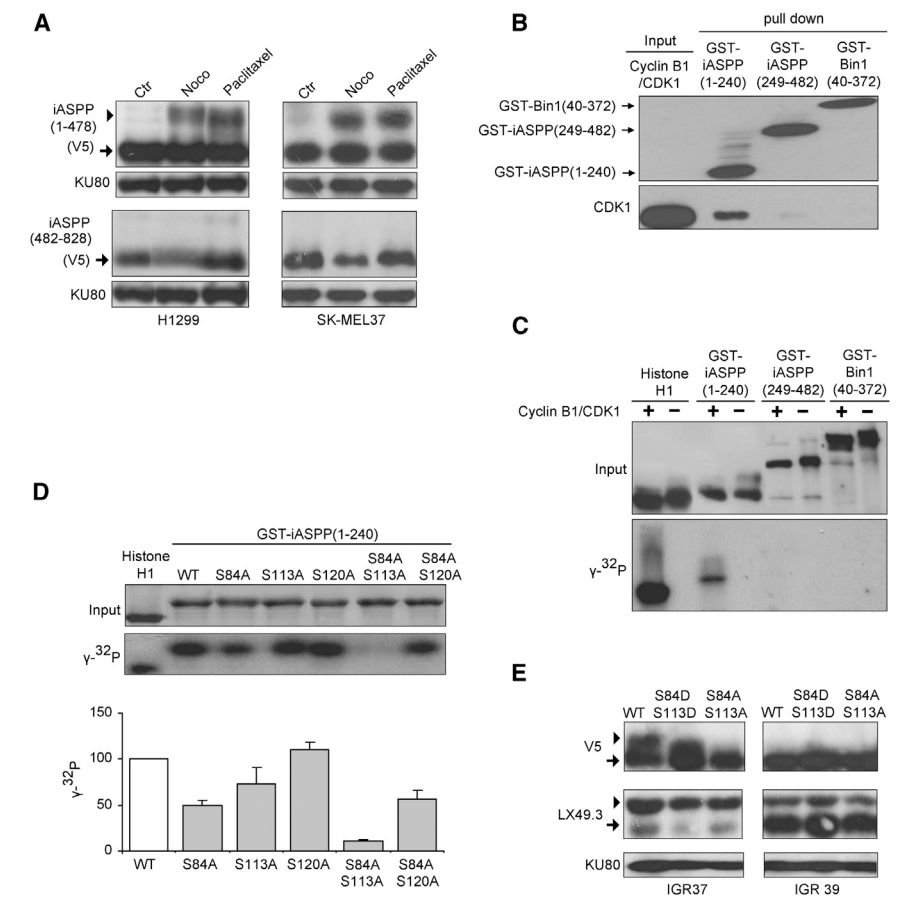
See also Figure S2.

similarity to iASPP's C terminus (Figure 4A). Using iASPP variants singly and doubly mutated at S84, S113, and S120 sites, it was seen that residues S84 and S113, but not S120, are involved in this N- and C-terminal interaction of iASPP, as Ala mutation of S84 and S113 weakened the interaction. Phosphorylation mimetic mutations S84D and S113D efficiently abrogated this interaction (Figure 4B).

Ras and E1A immortalized iASPP-deficient mouse embryonic fibroblasts (Ppp1r13I^{-/-} MEFs) were transfected with N-terminal iASPP(1-478) and treated with nocodazole to induce posttranslational modification and slow migration of transfected iASPP (1-478). The resulting lysates were incubated with purified recombinant iASPP C-terminal fragment, iASPP(625-828). iASPP(625-828) selectively bound nonmodified, fast-migrating N-terminal iASPP (Figure 4C). When purified recombinant iASPP(1-240) was incubated with nocodazole-treated H1299 lysates, it specifically bound to nocodazole-induced modified, slow-migrating endogenous iASPP with an exposed C terminus (Figure 4D).

In a denaturing SDS-PAGE gel, iASPP migrated as a single 100 kDa band in normal growing H1299 cells, but as double bands on nocodazole treatment. In a nondenaturing gel, iASPP from the same cells migrates as a single 250 kDa band. In nocodazole-treated H1299 cells, iASPP migrates as two bands differing in size (one \sim 110 kDa, the other 250 kDa), almost double the apparent size of fast-migrating iASPP (Figure 4E). Although this is not direct proof, the results suggest that in normal growing H1299 cells, iASPP may exist as an anti-parallel homodimer. Upon S84/S113 phosphorylation, the N- and C-terminal selfinteraction is disrupted, resulting in iASPP monomer formation.





Structural and sequence similarity between the two iASPP peptides, (GSPRKAAT, 83-90 aa) and (GSPRKARR, 615-622 aa) suggests that C-terminal T722, L724, N813, and Y814 might be contact residues for the N terminus (83-90 aa). Single and double mutants were generated on these four residues. iASPP(625-828)/T722A and iASPP(625-828)/L724A bound N-terminal iASPP slightly less efficiently than WT iASPP(625-828). iASPP(625-828)/N813A or iASPP(625-828)/Y814A had a much reduced ability to bind iASPP(1-240). iASPP(625-828)/ T722A/N813A, iASPP(625-828)/T722A/Y814A, iASPP(625-828)/L724A/N813A, and iASPP(625-828)/L724A/Y814A almost lost their ability to interact with iASPP(1-240) in pull-down assays. Mutant iASPP(625-828)S754A, which has a mutation outside the putative binding region, can fully interact with iASPP(1-240). This study identifies N813 and Y814 as two key residues that interact with N-terminal iASPP (Figures 4F and S4B).

To test whether N- and C-terminal self-interaction prevents iASPP nuclear entry, digitonin-permeabilized H1299 cells (with permeable cell membranes and intact nuclear membranes) were used for in vitro nuclear entry assays using-FITC labeled iASPP(625–828). FITC-labeled ASPP2(905–1128) was used as a negative control. Both C-terminal iASPP and ASPP2 can enter the nucleus with high efficiency (Sachdev et al., 1998; Slee et al., 2004). Preincubation with increasing amounts of nonlabeled N-terminal iASPP(1–240) prevented the nuclear entry of FITC-labeled iASPP(625–828). Under the same conditions, preincuba-

Figure 3. Phosphorylation of iASPP at S84/ S113 by Cyclin B1/CDK1 Contributes to iASPP Slow Migration

(A) Cells stably expressing iASPP(1-478)-V5 and iASPP(482-828)-V5 were treated with the indicated agents. iASPP fragments were detected by anti-V5 antibody.

(B) GST pull-down assay to detect the binding between Cyclin B1/CDK complex and purified GST-iASPP(1-240), GST-iASPP(249-482), or GST-Bin1 (40-372).

(C) Purified Histone H1 or GST-tagged proteins were incubated with cyclin B1/CDK1 complex and $[\gamma^{-32}P]$ -ATP in an in vitro kinase assay as indicated. $[\gamma^{-32}P]$ signal is shown in $\gamma^{-32}P$ panel.

(D) Purified GST-iASPP(1-240) or indicated mutants were subjected to cyclin B1/CDK1 in vitro kinase assay as for (C). Bar graph values are mean \pm SD of $\gamma^{-32}P$ signal from two independent experiments.

(E) IGR37 or IGR39 cells stably expressing V5-tagged wild-type or mutant iASPP were lysed and used to detect exogenous (V5 panel) and endogenous (LX49.3 panel) iASPP. See also Figure S3.

tion of iASPP phosphomimetic mutant iASPP(1–240)S84D/S113D failed to affect the nuclear entry efficiency of FITC-labeled iASPP(625–828). iASPP(1–240) affected the nuclear entry of iASPP(625–828) but not ASPP2(905–1128) (Figure 4G). iASPP(S84D/S113D)

showed more nuclear localization than WT iASPP and iASPP (S84A/S113A) in *Ppp1r13I*^{-/-} MEFs (Figure 4H). Nuclear localization of iASPP(S84A/S113A) and iASPP(S84D/S113D) was also observed in H1299 and WM278 cells, although differences in cellular distribution between iASPP and its mutants were less dramatic in these cells. Transfected iASPP expression patterns agreed with those of endogenous iASPP:iASPP-V5 was detected in both the cytoplasm and nucleus in WM278 cells, but mainly in the cytoplasm in H1299 (Figure S4C).

Phosphomimetic iASPP, iASPP(S84D/S113D), Is More Potent to Bind and Inhibit p53 Than WT iASPP

The abilities of iASPP and iASPP(S84D/S113D) to bind p53 were compared using in vitro translated iASPP and recombinant p53. Figure 5A shows that iASPP(S84D/S113D) binds p53 with greater affinity than iASPP in vitro. When transfected into p53 null H1299 cells, iASPP(S84D/S113D) also bound cotransfected p53 more effectively (Figure 5B). In Saos-2 cells, which are p53 null and express lower levels of iASPP than H1299 cells (Bergamaschi et al., 2006a), transfected iASPP(S84D/S113D) was more active than iASPP in inhibiting exogenous p53-mediated transcription on the promoters of p53 target genes *PIG3*, *BAX*, and *PUMA*. Neither iASPP nor iASPP(S84D/S113D) inhibited p53's transcriptional activity on the *CDKN1A*, which encodes p21^{CIP1} (Figure 5C). Similarly, iASPP(S84D/S113D) was more active than iASPP in inhibiting the transcriptional activity of endogenous p53 in MCF7 and



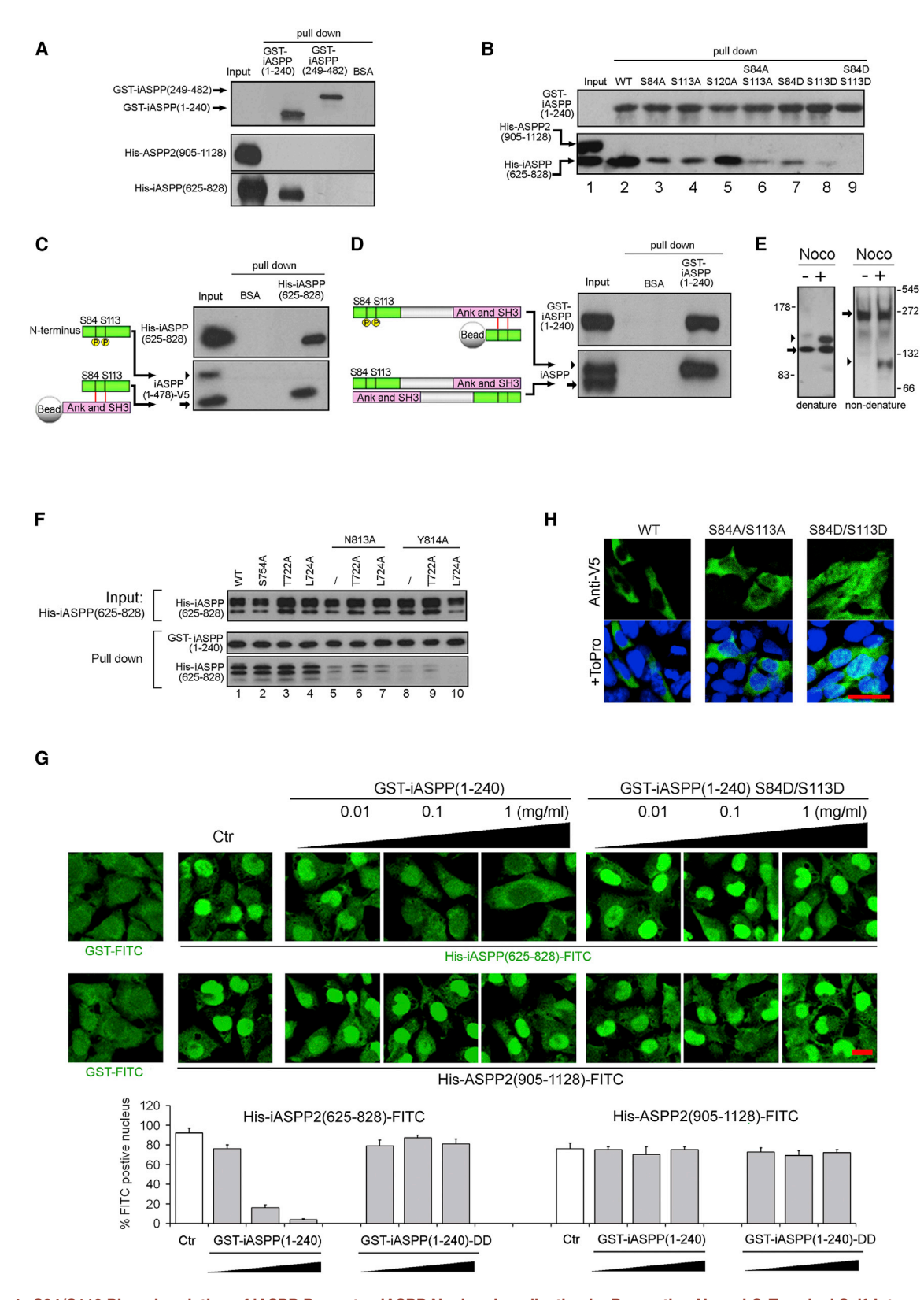


Figure 4. S84/S113 Phosphorylation of iASPP Promotes iASPP Nuclear Localization by Preventing N- and C-Terminal Self-Interaction (A) Purified GST-iASPP(1–240) or GST-iASPP(249–482) was incubated with purified His-iASPP(625–828) and His-ASPP2(905–1128), followed by GST pull-down assays

assays.

(B) Purified GST-iASPP(1–240) or mutants was incubated with purified His-iASPP(625–828) and His-ASPP2(905–1128), followed by GST pull-down assays.

(legend continued on next page)



B16 cells on *PIG3*, *BAX*, and *PUMA* but not *CDKN1A* promoters (Figure S5A and S5B).

Apoptosis was induced in both primary and immortalized Ppp1r13l^{-/-} MEFs by p53 inducers such as Nutlin3, UV, etoposide, or cisplatin. This was largely p53-dependent, as p53 RNAi abolished treatment-induced apoptosis (Figure S5C). iASPP and mutant iASPP(S84D/S113D) were introduced to immortalized Ppp1r13l^{-/-} MEFs competent in p53-mediated apoptosis. The presence of iASPP or iASPP(S84D/S113D) had little impact on cell survival in DMSO-treated cells. On treatment with Nutlin3, apoptosis was detected in immortalized Ppp1r13I^{-/-} MEFs transfected with control vector, based on an increase in c-caspase 3 (cleaved caspase 3 on D175) and decrease in procaspase 3. iASPP caused a minimal decrease in c-caspase 3 expression under these conditions. The presence of iASPP(S84D/S113D) resulted in a clear decrease in c-caspase 3 and a small increase in procaspase 3 levels, and caused the biggest reduction in the levels of c-caspase 3 in comparison to those detected in vector or iASPP-expressing cells exposed to 10 J/m² UV. Clear decreases in the expression of PIG3, BAX, and PUMA, but not CDKN1A, were observed in Ppp1r13I-/- MEFs expressing iASPP(S84D/S113D), compared to those expressing vector or iASPP (Figure 5D). Thus, iASPP(S84D/S113D) is more potent than iASPP in inhibiting apoptosis in response to Nutlin3 or UV

Wild-Type p53-Expressing Melanoma Cells Express High Levels of MDM2 and S84/S113 Phosphorylated Nuclear iASPP

To confirm that the observed alterations in iASPP's location and function are at least partly caused by modifications in the region containing S84 and S113, we generated mouse monoclonal antiiASPP antibody LX128.5 with an epitope mapped within the identified region (residues 81-130, Figure S6A). LX49.3 recognizes an iASPP epitope outside the modified region. Only fastmigrating cytoplasmic iASPP was recognized by LX128.5 (Figure 6A). Modification of iASPP on S84 and S113 destroys this epitope. Both nuclear and slow-migrating iASPP, as well as iASPP(S84D/S113D), lost the epitope recognized by LX128.5, which was previously recognized by LX49.3 (Figures S6B and S6C). Comparing this to the expression patterns of iASPP in the same panel of 18 melanoma lines (Figure S6D), we concluded that slow-migrating iASPP detected by LX49.3 lost the LX128.5 epitope. Slow-migrating iASPP detected in this panel of cell lines is thus likely to be phosphorylated nuclear iASPP, modified in the region that contains S84 and S113.

To test whether cyclinB/CDK1-phosphorylated nuclear iASPP contributes to p53 inactivation in melanomas, the panel of 18

lines used above was analyzed for iASPP, p53, and cyclin B1 expression. In contrast to human primary melanocytes, iASPP, MDM2, and cyclin B1 are overexpressed in most melanoma lines. Increased expression of MDMX and p53 was detected in some lines, whereas CDK1 expression was more constant (Figure 6B). Of note, 91% (10/11) of WT p53-expressing melanoma lines expressed a high proportion of phosphorylated iASPP (>50%), whereas 86% (6/7) of those expressing mutant p53 had a lower proportion (<20%, Figure 6B). Approximately 80% (9/11) of WT p53-expressing lines had detectable to high levels of MDM2, whereas only 45% expressed detectable MDMX (5/11) under the same conditions. Approximately 70% of the WT p53 lines expressed relatively high levels of MDM2 and phosphorylated nuclear iASPP, many of which also expressed relatively high levels of cyclin B1. Levels of phosphorylated iASPP were not linked to the expression levels of other cell cycle regulating proteins such as CDK1, CDK2, cyclin A, cyclin E, p16, p21, or p27 (Figures S6E and S6F). Elevated phosphorylated iASPP expression was not due to an increase in mitosis, as the expression levels of phosphohistone H3 were almost constant among most of the cell lines tested, and differed from cyclin B1 levels (Figure S6F). The percentage of G2/M cells detected in the panel of melanoma lines did not correlate with levels of cyclin B1 or iASPP modification, although high levels of cyclin B1 associated with high levels of modified iASPP (Figures S6G and S6H).

Consistent with this in vitro finding, we observed that weak cyclin B1 and cytoplasmic iASPP, or strong cyclin B1 and high nuclear iASPP expression, often occur in the same human melanoma samples (Figures 6C and 6D). To investigate the correlation of cyclin B1 and nuclear iASPP in primary tumors and metastases, samples were divided into six groups as indicated (Figures 6E and 6F). Weak cyclin B1 and low nuclear iASPP expression was observed in ~81% of primary melanomas (26/32), whereas ~83% express strong cyclin B1 and high nuclear iASPP in lymph node metastases (5/6) (Figure 6E). In a cohort of 66 melanoma patients, high nuclear iASPP was significantly associated with poor survival. A trend to association of high cyclin B1 with poor survival was seen, but a larger independent cohort is needed to conclude whether strong cyclin B1+nuclear iASPP is associated with the worst survival outcome (Figure 6F).

Restoring p53 by Inhibiting MDM2 and iASPP Suppresses Melanoma Growth In Vitro and In Vivo

Knocking down cyclin B1 with RNAi abolished slow-migrating iASPP in the presence of nocodazole (Figure 7A). Increased expression of cyclin B1, but not CDK1, induced nuclear localization of iASPP in H1299 cells, agreeing with the fact that CDK1 is in excess in cells, cyclin B1 dictates the kinase activity of cyclin

⁽C) Ras + E1A transformed *Ppp1r13I*^{-/-} MEFs stably expressing iASPP(1–478)-V5 were treated with nocodazole for 16 hr. Cell lysates were mixed with purified His-iASPP(625–828) and subjected for His pull-down assays.

⁽D) H1299 cells were treated with nocodazole for 16 hr. Cell lysates were mixed with purified GST-iASPP(1-240) and subjected for GST pull-down assays.

⁽E) iASPP migration from DMSO- or nocodazole-treated H1299 cells was determined in denaturing or nondenaturing gels as indicated.

⁽F) Purified His-iASPP(625–828) or mutants were mixed with GST-iASPP(1–240), followed by GST pull-down assay.

(G) Purified His-iASPP(625–828)-FITC or His-ASPP2(905–1128)-FITC were preincubated without (Ctr) or with increasing amounts of GST-iASPP(1–240) or GST-iASPP(1–240)S84D/S113D as indicated, and applied to digitonin-treated H1299 cells. Scale bar represents 20 μm. Bar graph (mean ± SD) shows percentage of FITC-positive nuclei after treatment derived from three independent experiments. Greater than 100 cells were counted.

⁽H) Immunofluorescence staining of stably expressed iASPP mutants (V5 tagged) in Ras + E1A transformed *Ppp1r13l*^{-/-} MEFs. Scale bar represents 20 μm. See also Figure S4.



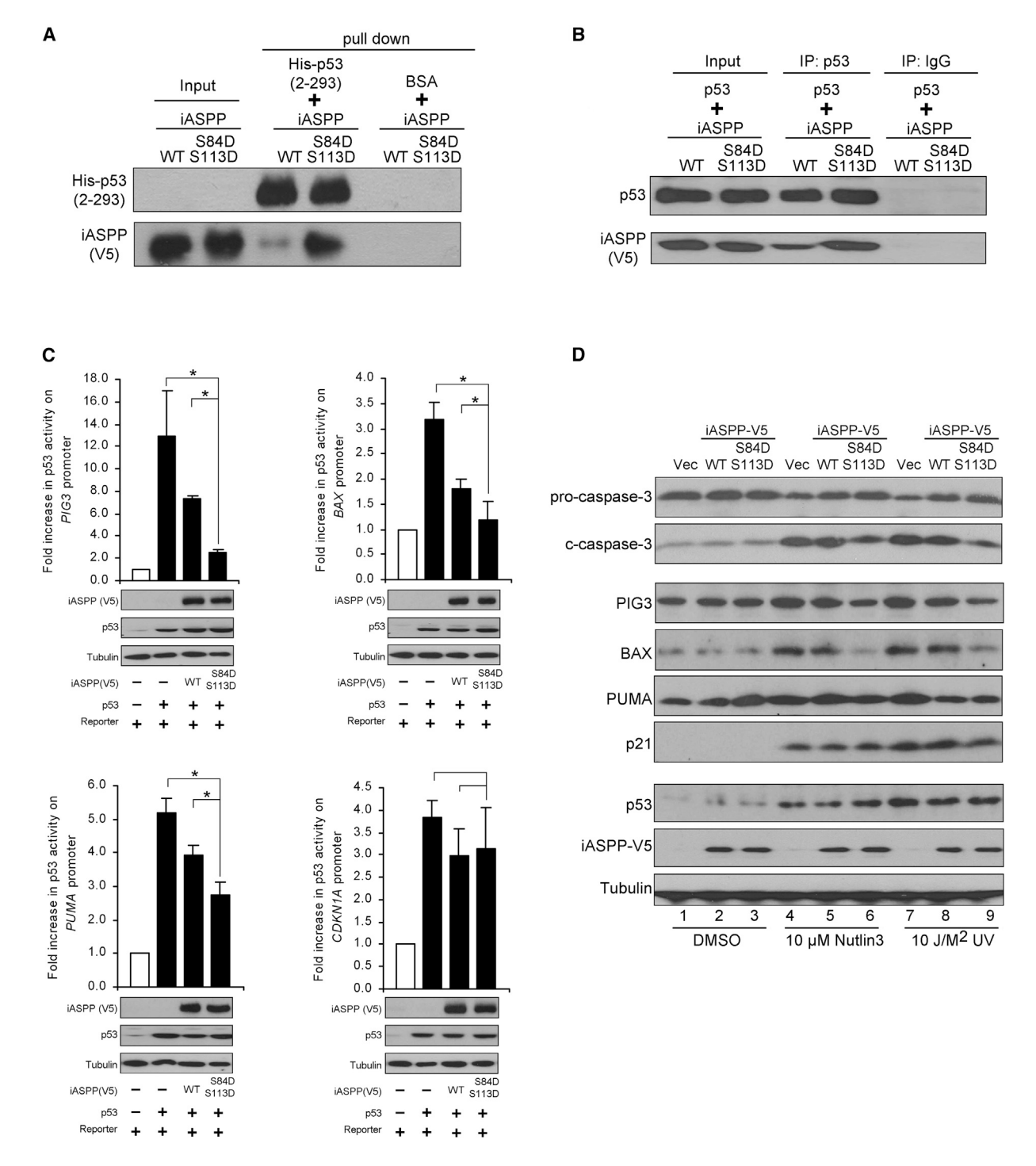


Figure 5. Phosphomimetic iASPP, iASPP(S84D/S113D), Is a More Potent Binder and Inhibitor of p53 Than WT iASPP

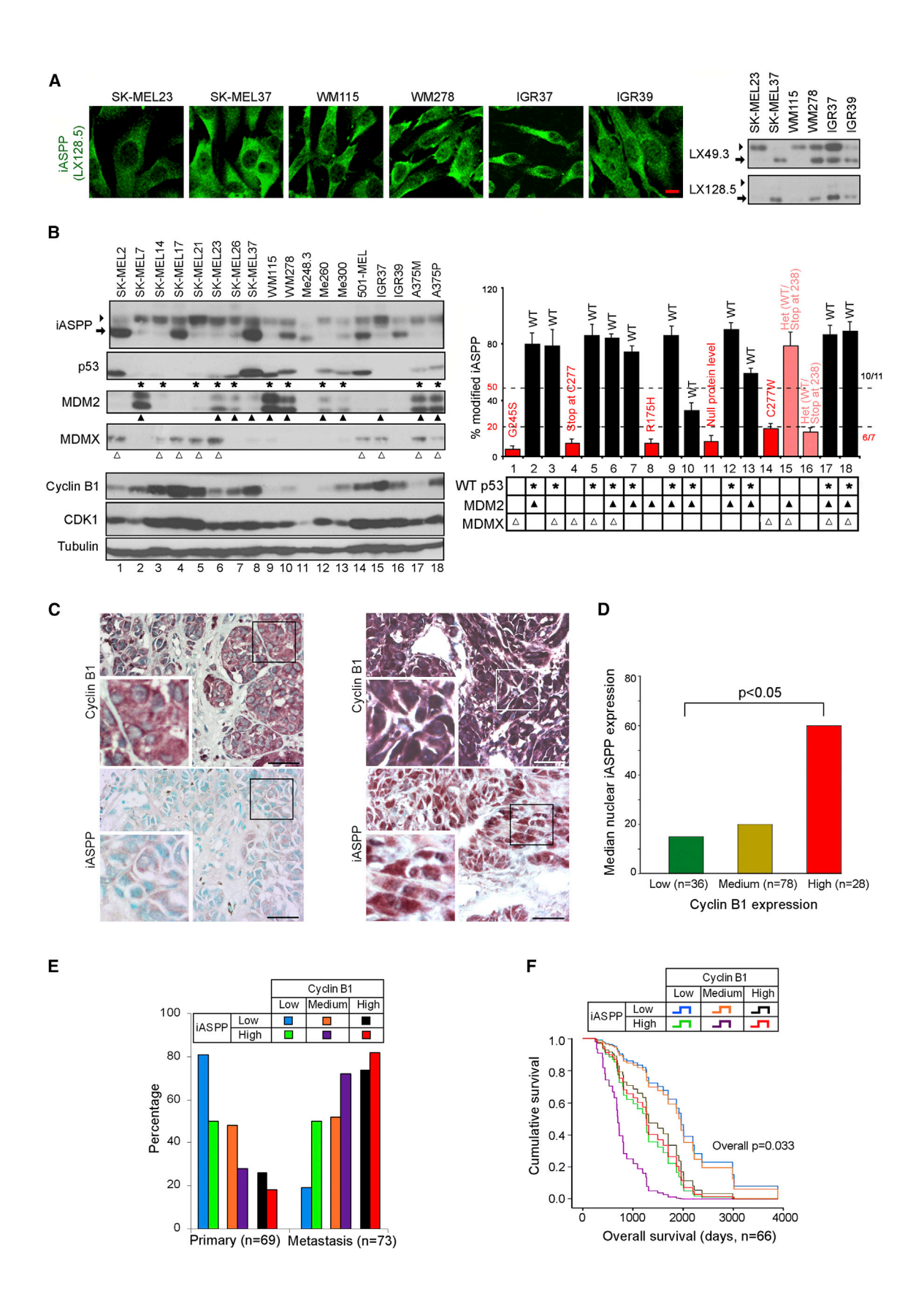
(A) His-p53(2-293) and in vitro-translated iASPP-V5 (WT) or iASPP(S84D/S113D)-V5 (S84D/S113D) in a His pull-down assay. BSA was used as a negative control.

(B) iASPP-V5 (WT) or iASPP(S84D/S113D)-V5 (S84D/S113D) and p53 were cotransfected in H1299 cells (input), followed by coimmunoprecipitation using p53

(C) Effects of iASPP (WT) or iASPP(S84DS113D) on the transcriptional activity of exogenous p53 in Saos-2 cells measured using a panel of reporters containing the promoter of PIG3, BAX, PUMA, or CDKN1A. Bar graph shows mean ± SD from three independent experiments (*p < 0.05). Lower panels: expression levels of transfected iASPP and p53 are indicated.

(D) Ras + E1A transformed Ppp1r13I^{-/-} MEFs stably expressing vector (Vec), iASPP(WT), or iASPP(S84D/S113D) (S84D/S113D) were subjected to various treatments for 24 hr as indicated. Protein levels of cleaved caspase 3 (c-caspase 3) and p53 targets were detected by immunoblotting. See also Figure S5.







B1/CDK1 (Figure 7B). A panel of 15 G2/M kinase inhibitors was tested for their ability to prevent nocodazole-induced iASPP modification in H1299 cells. At 2–10 μM concentrations, most inhibitors against Aurora kinase, Polo like kinase (PLK), Pim1, or Mps1 kinase failed to abrogate nocodazole-induced iASPP modification (Figures 7C and S7A). In contrast, several inhibitors known to affect cyclin B/CDK1 activity inhibited iASPP modification. The most potent inhibitor of iASPP modification in the presence of nocodazole was JNJ-7706621 (JNJ), a CDK1 inhibitor with an in vitro IC₅₀ of 9 nM for cyclin B/CDK1 (Emanuel et al., 2005). The CDK2 inhibitor Roscovitine only weakly affected iASPP modification (Figures 7C and S7A). To provide supporting evidence that p53 selectively binds cyclin B1/CDK1-phosphorylated nuclear iASPP, WM278 cells were treated with DMSO, nocodazole, or JNJ, and treated cell lysates incubated in the presence or absence of a Ser/Thr phosphatase (calf intestine alkaline phosphatase [CIP]) before immunoprecipitation. JNJ alone reduced the amount of modified iASPP, whereas nocodazole increased it. CIP treatment abolished nocodazole-induced iASPP modification. p53 failed to coimmunoprecipitate iASPP in JNJ, control+CIP- and nocodazole+CIP-treated lysates, although it was efficiently coimmunoprecipitated with modified iASPP in both control and nocodazole-treated WM278 cells (Figure 7D). These data illustrate that p53 selectively binds phosphorylated iASPP in vivo.

Cells were treated with various concentrations of Nutlin3 to identify concentrations that induce maximal p53 expression (Figures S7B and S7C). The ability of JNJ to reactivate WT p53 function was also tested in a panel of 11 melanoma lines in which the mutation status of p53, NRAS, and BRAF were confirmed by sequencing. When WT p53, NRAS, and BRAFV600E-expressing WM278 cells were treated with Nutlin3 or JNJ alone, a small percentage of apoptotic cells were induced with limited cell growth suppression, despite induction of p53 expression. However, iASPP RNAi or JNJ resulted in significant increases in Nutlin3-induced apoptosis, determined by the presence of cells expressing Annexin V (Figure 7E) and colony formation assay (Figure 7F) or containing Sub-G1 DNA (Figure S7D). Apoptosis induced by JNJ+Nutlin3 was iASPP and p53-dependent: in the presence of iASPP RNAi, JNJ failed to further enhance Nutlin3-induced apoptosis. p53 RNAi largely prevented both apoptosis and growth suppression induced by JNJ+Nutlin3. The synergistic effects of JNJ and Nutlin3 in inducing apoptosis and suppressing colony formation were observed in an additional nine WT p53-expressing melanoma lines, but not mutant p53-expressing SK-MEL37 cells (Figures S7E-S7H). The observed synergistic effects of JNJ and Nutlin3 are largely iASPP- and p53-dependent, regardless of BRAF mutation.

The identified regulation of p53 by iASPP and MDM2 exists in both human WM278 and mouse B16 melanoma cells. We thus tested whether restoring p53 function is able to suppress the growth of highly aggressive B16 melanomas in immune competent C57BL/6 syngeneic mice. B16 cells treated with DMSO, Nutlin3, JNJ, and Nutlin3+JNJ were injected into the flanks of C57BL/6 mice and tumors analyzed after 13 days. Tumors derived from JNJ-, Nutlin3-, or JNJ+Nutlin3-treated B16 cells were around 34%, 59%, or 14% of those derived from the DMSO group, respectively. JNJ treatment appears more potent in inhibiting B16 growth in vivo than in colony assays (Figures 7G and 7H). The underlying cause of this discrepancy is unknown.

The ability of Nutlin3+JNJ to inhibit B16 melanoma growth in vivo was further tested by inoculating untreated B16 cells into C57BL/6 mice, 3 days (Figures S7I-S7K) or 7 days (Figures 7I-7K) prior to intraperitoneal administration of DMSO, Nutlin3 (40 mg/kg), JNJ (30 mg/kg), or Nutlin3+JNJ every 2 days as indicated. Treatment with Nutlin3+JNJ suppressed tumor weight/ size of B16 melanomas by 61%-66% compared to DMSO. Administration of Nutlin3 from day 3 or 7 after B16 inoculation suppressed melanoma growth by 22% or 5%, but injection of JNJ at both time points suppressed melanoma growth by 36% or 30%, respectively (Figures 7J and S7J). These data suggest that the timing of MDM2 inhibition may affect Nutlin3 efficacy, but the efficacy of JNJ or JNJ+Nutlin3 is less affected by first administration time.

Both cytoplasmic and nuclear iASPP were detected in DMSOtreated B16 tumors (Figure 7K). Under the same conditions, p53 expression was almost undetectable. Treatment with JNJ clearly reduced nuclear iASPP expression in a number of B16 tumor cells but had no effect on p53 expression. Nutlin3 treatment induced nuclear p53 expression and had minimal impact on iASPP expression. Treatment with JNJ+Nutlin3 resulted in a reduction in nuclear iASPP and an increase in nuclear p53 (Figure 7K). This illustrates that JNJ's tumor suppressive effect associates with reduced nuclear iASPP expression in B16 tumor cells in vivo. Combined treatment with JNJ and Nutlin3 restores the p53's tumor suppressive function and inhibits melanoma growth in vivo.

Restoring the Apoptotic Function of p53 Cooperates with BRAFV600E Inhibition to Suppress Human Melanoma Cell Growth In Vitro and In Vivo

To examine whether restoring WT p53 function and concurrently inhibiting BRAFV600E has cooperative effects, WM278, Me300, A375P, and SK-MEL37 were treated with increasing amounts of vemurafenib. One micromolar of vemurafenib was identified as the optimal concentration to induce apoptosis in these cells

Figure 6. WT p53-Expressing Melanoma Cells Express High Levels of MDM2 and S84/S113 Phosphorylated Nuclear iASPP

(A) Immunofluorescence staining and immunoblot to show iASPP cellular localization and mobility in indicated cells. Scale bar represents 20 µm. Lx49.3 or LX128.5 as indicated were used for iASPP detection.

(B) Lysates from indicated melanoma cell lines were immunoblotted with indicated antibodies. The bar graph shows the percentage of iASPP modification (mean ± SD from two independent experiments) and p53 status (indicated on the bar). Cell lines with WT p53, overexpressed MDM2, or overexpressed MDMX were labeled with stars, triangles, and hollow triangles, respectively.

(C-F) Analysis in 142 human melanoma tissue array cores. Two representative iASPP and cyclin B1 staining. Scale bar represents 50 µm (C). The median nuclear iASPP expression levels in samples that expressing low, medium, or high cyclin B1 (U = 340.500, r = -0.28, p < 0.05) (D). Percentage of samples expressing various cyclin B1 levels and nuclear iASPP levels from lymph node metastases and primary tumors, respectively (E). Survival curve of patients expressing various cyclin B1 levels and nuclear iASPP levels (F).

See also Figure S6.



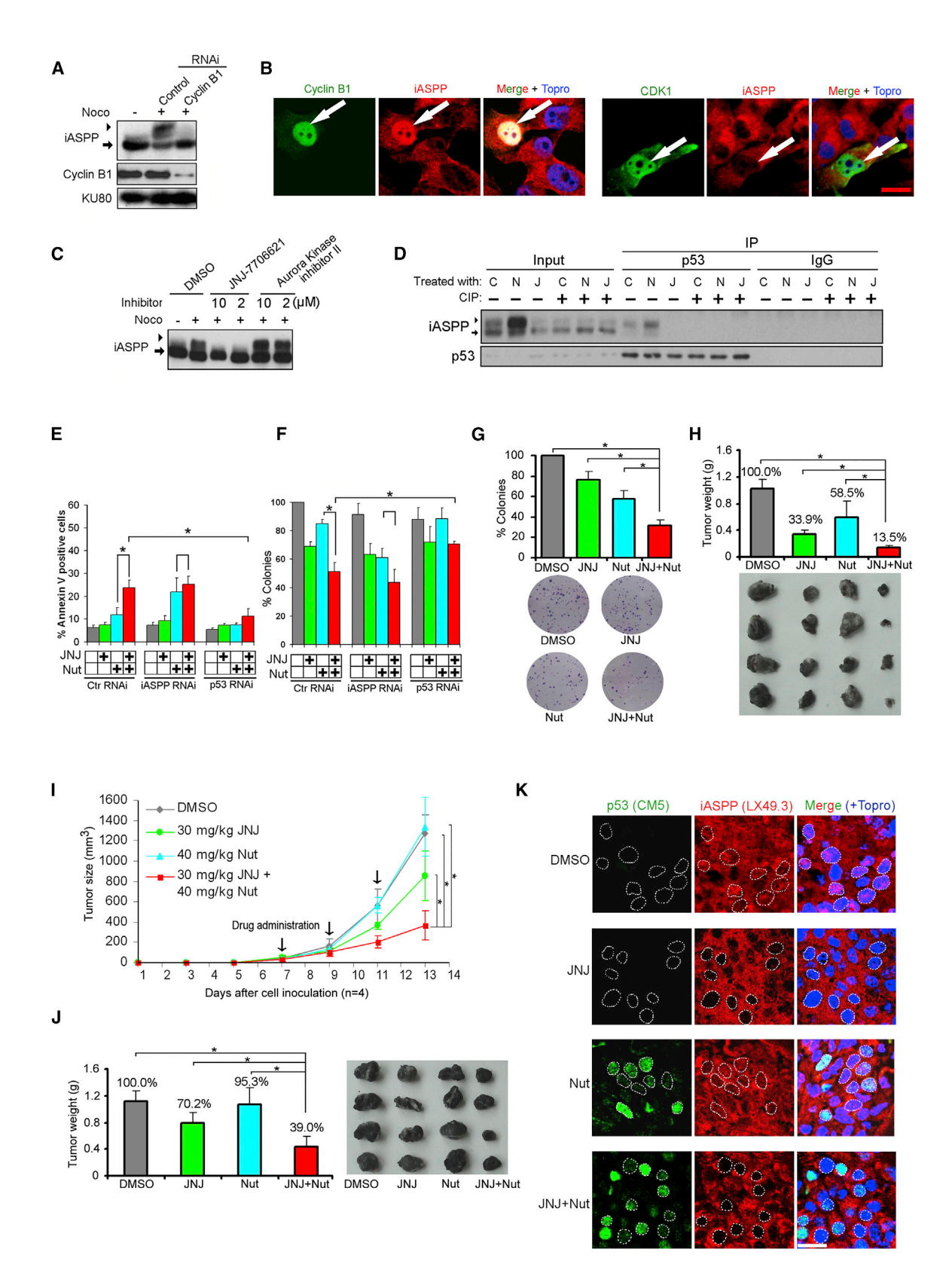


Figure 7. Restoring p53 by Inhibiting MDM2 and iASPP Suppresses Melanoma Growth In Vitro and In Vivo
(A) Immunoblot of iASPP in H1299 cells treated with cyclin B1 RNAi in the presence or absence of 10 μM nocodazole.
(B) Immunofluorescence staining shows localization of transfected cyclin B1 or CDK1 and endogenous iASPP in H1299 cells. Cells expressing transfected cyclin B1 or CDK1 are labeled by white arrows. Scale bar represents 20 μm.



(Figure S8A and data not shown). The highest levels of apoptosis (Figures 8A and S8B) and growth suppression (Figures 8B and S8C) were observed in WM278 cells when JNJ, Nutlin3, and vemurafenib were used together to induce the expression of proapoptotic genes such as BAX and PUMA (Figure S8D; note that the results in Figures 7E and 7F were controls for Figures 8A and 8B, hence part of Figures 8A and 8B are identical to that of Figures 7E and 7F). Vemurafenib alone induced apoptosis and growth suppression in WM278 cells, possibly achieved by inhibiting McI-1 expression (Figure S8D). Similar results were obtained in BRAFV600E-expressing A375P, Me300, and SK-MEL26 cells, but not the panel of WT BRAF-expressing cells (Figures S8E and S8F). MEK is a direct downstream kinase of BRAF. Interestingly, MEK inhibitor U0126 cooperated with JNJ+Nutlin3 in inducing apoptosis and growth suppression to a similar extent as vemurafenib. No additive effect was observed between vemurafenib and U0126 (Figures 8C, 8D, and S8G).

The therapeutic potential of the combination of vemurafenib, JNJ, and Nutlin3 was tested using the A375P human melanoma xenograft model. A375P cells treated with DMSO, Nutlin3, JNJ, and Nutlin3+JNJ in the presence or absence of vemurafenib were injected into the flanks of nude mice for 28 days. Experiments were terminated when tumors reached 1 cm in diameter in the DMSO-treated group. Tumors derived from Nutlin3-, JNJ-, or JNJ+Nutlin3-treated A375P cells were 1%, 30%, or 58% smaller than those from the DMSO group, respectively (Figures 8E and 8F). Tumors derived from vemurafenib, Vem+Nut, Vem+JNJ, and Vem+JNJ+Nut were 39%, 40%, 59%, and 75% smaller, respectively.

A375P cells were inoculated into nude mice for 10 days to develop visible tumors prior to the administration of various combinations of compounds. Intraperitoneal injection of the indicated combinations of 20 mg/kg vemurafenib, 30 mg/kg JNJ, and 40 mg/kg Nutlin3 had no visible impact on animal health and weight loss (Figure S8H). Importantly, injection of Nut+JNJ or Nut+JNJ+Vem suppressed A375P melanoma growth by \sim 58% and \sim 88% in size (Figure 8G) and \sim 67% and \sim 88% in weight (Figure 8H) compared to DMSO controls. Under the same conditions Nutlin3, JNJ, or vemurafenib injection alone only inhibited A375P melanoma growth by 4%, 41%, and 51% in weight, respectively. Coinjection of Vem+JNJ or Vem+Nut achieved similar growth suppression, inhibiting tumor growth by \sim 66% or \sim 69% in weight (Figure 8H). Finally, immunofluorescent staining confirmed that intraperitoneal injection of JNJ can reduce nuclear iASPP expression, whereas Nutlin3 induces p53 expression in A375P melanoma cells in vivo (Figure S8I). These data show that restoring the apoptotic function of p53, together with BRAFV600E inhibition, can achieve additive effects in suppressing melanoma growth in vitro and in vivo.

DISCUSSION

Here, we show that p53 is inhibited by cyclin B1/CDK1-phosphorylated nuclear iASPP, in addition to MDM2, in the majority of wild-type p53-expressing melanomas (Figure 8I). The tumor suppressive function of p53 in melanomas can be restored by concurrently inhibiting both MDM2 and iASPP phosphorylation, using Nutlin3 and JNJ, respectively, both in vitro and in vivo. Our results further suggest that targeting two independent pathways may represent a promising melanoma treatment strategy (Figure 8J).

The action of JNJ contrasts with a recent finding that Nutlin3 specifically cooperates with VX-680, an Aurora kinase inhibitor, to kill mutant, but not WT p53-expressing, cells (Cheok et al., 2010). The observed specificity of JNJ and VX-680 for WT and mutant p53 is intriguing. The selective impact of JNJ on WT p53 when combined with Nutlin3 may be linked to the phosphorylation of iASPP at SP sites favored by CDK family kinases (Johnson, 2011). Aurora, Plk1, Pim1, and Msp1 do not efficiently phosphorylate SP sites, and inhibitors of Aurora, Plk1, Pim1, and Msp1 kinases failed to inhibit nocodazole-induced iASPP modification. Several phosphoproteome studies have identified phosphorylation of iASPP on S102, S110, S119, and S120, in the region that interacts with iASPP's C terminus. Phosphorylation on multiple sites may thus be responsible for the large mobility shift observed. However, the ability of iASPP(S84A/ S113A) to abrogate slow-migrating iASPP in IGR37 cells, which express slow-migrating endogenous iASPP, suggests that S84 and S113 are the two key phosphorylation sites required to initiate or prime other iASPP modifications.

The observed regulation of iASPP's self-interaction and localization is p53-independent. However, both p53 and iASPP are substrates of cyclin B1/CDK1. Phosphorylation of p53 at Ser315 by cyclin B1/CDK1 or cyclin A/CDK2 in human and Ser312 in mouse contributes to the apoptotic and tumor suppressive function of p53 in vitro and in vivo (Fogal et al., 2005; Slee et al., 2010; Wang and Prives, 1995). Hence phosphorylation of p53 may regulate iASPP/p53 interaction and p53's function in G2/M. iASPP is also able to bind and regulate the p53 family members p63 and p73 (Bell and Ryan, 2008; Notari et al., 2011). Thus, the observed regulation of iASPP/p53 interaction is likely to apply to p63 and p73. Very little is known about p63 in human melanomas, but p73 was reported to play an important role in mutant p53-expressing melanoma cells (Rudolf

⁽C) Immunoblot of iASPP in H1299 cells treated with indicated compounds for 16 hr.

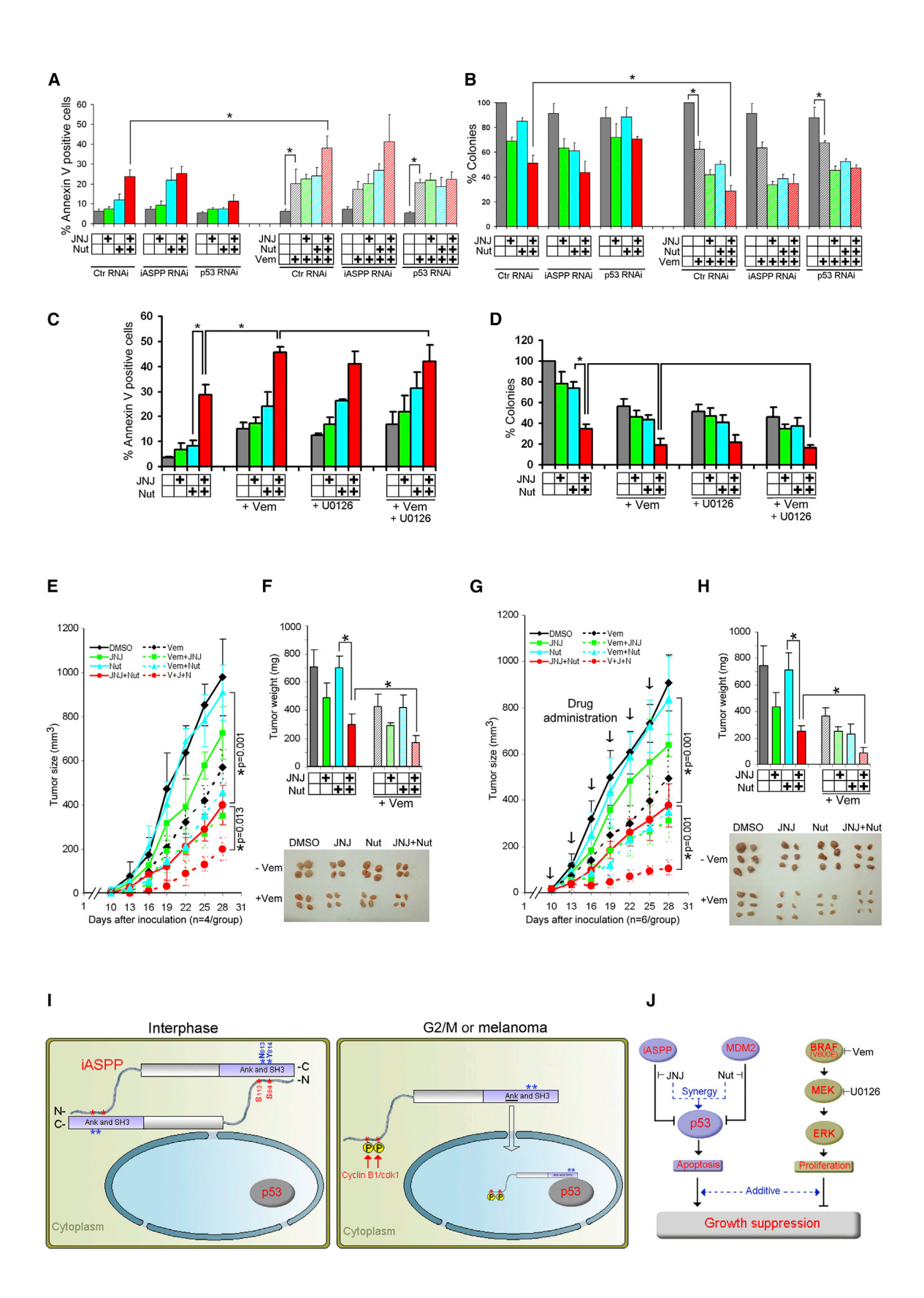
⁽D) WM278 cells treated with DMSO (C), 0.4 μ M JNJ (J), or 10 μ M nocodazole (N) for 16 hr were lysed and incubated with (+) or without (-) calf intestine alkaline phosphatase (CIP) for 1 hr, followed by p53 coimmunoprecipitation.

⁽E and F) WM278 cells were treated with JNJ, Nutlin3, or a combination in the presence or absence of control, iASPP and p53 RNAi, as indicated. Bar graphs show percentage of Annexin V positive cells (E) and percentage of treated cells that formed colonies (F). Bar graphs (mean ± SD) were derived from three independent experiments. *p < 0.05.

⁽G and H) Colonies (G) and tumors (H) formed from treated B16 cells as indicated. Bar graphs show mean ± SD (*p < 0.05, n = 4/group).

⁽I-K) Untreated B16 cells were subcutaneously injected into flanks of mice at day 1. Indicated compounds were intraperitoneally injected on day 7. Compound administration (indicated by arrows) and tumor size measurement (I) was repeated every 2 days from day 7 onward. Weights (J) and immunofluorescence staining of iASPP and p53 (K) of tumors on day 13. Graphs of show mean ± SD (*p < 0.05, n = 4/group). White dotted circles in (K) show representative nuclear rim derived from Topro staining. Scale bar represents 20 μm .







et al., 2011). Future studies are needed to explore how iASPP/ p63 and iASPP/p73 interaction is regulated, and whether it can influence p63- and p73-mediated cell cycle progression and genome stability.

A whole genome-based array showed that cyclin B1 was highly upregulated in human melanoma cells (Avery-Kiejda et al., 2011). Increased cyclin B1 protein levels were also reported in metastatic melanoma tissue sections compared to primary melanomas (Georgieva et al., 2001). Increased cyclin B1 expression is not limited to melanomas, and was detected in esophageal squamous cell carcinomas that contribute to metastasis (Song et al., 2008). These studies corroborate our finding that nuclear iASPP is significantly associated with metastatic melanoma. Deregulation of cyclin B1/CDK1 and increased iASPP S84 and S113 phosphorylation are likely to occur in other tumor types. Hence JNJ+Nutlin3 may reactivate p53 in other WT p53-containing tumors expressing high levels of cyclin B1. Restoration of WT p53 function and inhibition of BRAFV600E represents a means of enhanced cell killing in human melanoma. Strategies that target both p53-dependent and -independent pathways to inhibit cell growth or induce cell death may be fertile grounds for synergistic killing of the 50% of tumor cells that express WT p53.

EXPERIMENTAL PROCEDURES

Plasmids, Antibodies, Cell Lines, Compounds and Mice See Supplemental Experimental Procedures.

Immunoprecipitation, Pull-Down, Immunoblotting, Cell Shake-Off, and In Vitro Cyclin B1/CDK1 Kinase Assay

Cells were lysed in NP40 buffer for immunoprecipitation or 8 M urea buffer for immunoblotting. For pull-down assays, beads preincubated with purified Hisor GST-tagged proteins were mixed with 450 µl NP40 buffer containing either $5 \mu g/ml$ purified proteins or 2 mg/ml cell lysate.

 $H1299, WM278, or \, melanocytes \, were \, preseeded \, in \, T175 \, flasks \, for \, 16 \, hr \, and \,$ heavily shaken five times. Floating and adherent cells were collected. iASPP expression was detected by immunoblotting or immunofluorescence staining after cytospin. Recombinant N-terminal iASPP and its mutants were incubated with cyclin B1/CDK1 complex in a kinase assay mixture for 10 min at room temperature (RT). See Supplemental Experimental Procedures for details.

Mass Spectrometry, FITC Conjugation, and In Vitro Nuclear Import Assav

H1299 cells were grown and lysed in NP40 buffer. Protein lysate (40 mg) was immunoprecipitated with 100 μ l crosslinked LX49.3-proteinG Sepharose beads before SDS-PAGE. Isolated gel bands were subjected to trypsin digestion and HPLC purification before 3D high capacity ion trap mass spectrometer analysis.

Purified GST, His-iASPP(625-828), or His-ASPP2(905-1128) were conjugated with FITC. In vitro nuclear import assays were carried out as described (Van Impe et al., 2008). See Supplemental Experimental Procedures for

p53, BRAF, NRAS Sequencing, Transactivation Assay, and Knock Down of Cyclin B1, p53, and iASPP

mRNA and genomic DNA were extracted from all melanoma cell lines. TP53, BRAF, and NRAS were amplified by PCR and the products sequenced.

Cells plated in 12-well plates were transfected with 250 ng of luciferase reporter plasmid, 50 ng of p53, and 100 ng of iASPP expression plasmids per well as indicated. Luciferase reporter activities were detected using a luciferase assay kit (Promega).

siRNA of cyclin B1, p53, or iASPP was reverse transfected into cells using DharmaFECT 1 Transfection Reagent kit. See Supplemental Experimental Procedures for details.

FACS Analysis, Colony Formation, and Xenograft Assay

Cells were incubated with either DMSO or 0.4 μM JNJ for 48 hr to block iASPP modification. Cells were digested and transfected with siRNA using DharmaFECT 1 Transfection Reagent kit and seeded on 6-well plates in fresh medium containing DMSO, 0.4 μ M JNJ, 10–20 μ M Nutlin3, 1–5 μ M vemurafenib, or indicated combinations for 72 hr. Treated cells were collected and used for immunoblotting, FACS analysis, or colony formation. Cells $(1-5 \times 10^6)$ treated as above were used for mouse xenograft assay. All animal experiments were approved by the animal use ethical committee of Oxford University and fully complied with UK Home Office guidelines. See Supplemental Experimental Procedures for details.

Characterization of Anti-iASPP Antibodies, Immunohistochemistry Staining, and Patient Survival Analysis

Human iASPP(1-240) was used to immunize mice and a panel of mouse monoclonal anti-iASPP antibodies characterized as described previously (Fredersdorf et al., 1996; Slee et al., 2004). Melanoma tissue arrays were used to detect iASPP or cyclin B1 expression using immunohistochemistry staining (Notari et al., 2011). A multivariate Cox proportional hazards model was used to analyze the association between high levels of nuclear iASPP and patient survival. Experimental work on the clinical tissue used in this study was conducted under approval from the Oxfordshire Research Ethics Committee C (09/H0606/5). Written informed consent was obtained from all subjects whose tumor tissue was used in this study. See Supplemental Experimental Procedures for details.

SUPPLEMENTAL INFORMATION

Supplemental Information includes eight figures and Supplemental Experimental Procedures and can be found with this article online at http://dx.doi. org/10.1016/j.ccr.2013.03.013.

Figure 8. Restoring the Apoptotic Function of p53 Cooperates with BRAFV600E Inhibition to Suppress Human Melanoma Cell Growth In Vitro and In Vivo

(A and B) Bar graphs show the percentage of Annexin V positive cells (A) and percentage of treated cells that formed colonies (B) in WM278 cells treated with 0.4 µM JNJ, 20 µM Nutlin3, 1 µM vemurafenib, or combinations in the presence of control, iASPP, or p53 RNAi as indicated. Bar graphs (mean ± SD) were derived from three independent experiments. *p < 0.05.

(C and D) Bar graphs show the percentage of Annexin V positive cells (C) and percentage of treated cells that formed colonies (D) in A375P cells treated with 0.4 μM JNJ, 10 μM Nutlin3, 1 μM vemurafenib, 2 μM U0126, or combinations. Bar graphs (mean ± SD) were derived from two independent experiments. *p < 0.05. (E and F) In vitro-treated A375P cells were subcutaneously injected into flanks of nude mice on day 1. Tumor size measurement was repeated every 3 days (E). Mice were culled on day 28 and isolated tumors weighed (F). Graphs show mean ± SD (*p < 0.05, n = 4/group). Lower panel shows tumors derived.

(G and H) Untreated A375P cells were subcutaneously injected into flanks of nude mice at day 1. Indicated compounds administration (marked by arrows) and tumor size measurement (G) was repeated every 3 days from day 10 onward. Mice were culled on day 28 and isolated tumors weighed (H). Graphs show mean ± SD (*p < 0.05, n = 6/group). Lower panel shows tumors derived.

(I) Schematic diagrams showing cyclin B1/CDK1 phosphorylation controls iASPP localization in interphase (interphase) or in G2/M cells (or melanoma cells). Blue and red stars (*) indicate the C- and N-terminal contacting residues.

(J) Schematic diagrams showing JNJ, Nut, and Vem synthetically suppress melanoma growth. See also Figure S8.



ACKNOWLEDGMENTS

This work was funded by the Ludwig Institute for Cancer Research. We thank Evelyn Harvey and Dr. Claire Beveridge for critical reading of the manuscript. M.R.M. and B.M.K. are supported by the Oxford NIHR Biomedical Research Centre. S.K. is supported by the Structural Genomics Consortium (SGC). N.B. and J.E. are supported by the Medical Research Council, UK.

Received: April 5, 2012 Revised: October 5, 2012 Accepted: March 15, 2013 Published: April 25, 2013

REFERENCES

Avery-Kiejda, K.A., Bowden, N.A., Croft, A.J., Scurr, L.L., Kairupan, C.F., Ashton, K.A., Talseth-Palmer, B.A., Rizos, H., Zhang, X.D., Scott, R.J., and Hersey, P. (2011). P53 in human melanoma fails to regulate target genes associated with apoptosis and the cell cycle and may contribute to proliferation. BMC Cancer 11, 203.

Bell, H.S., and Ryan, K.M. (2008). iASPP inhibition: increased options in targeting the p53 family for cancer therapy. Cancer Res. 68, 4959–4962.

Bergamaschi, D., Samuels, Y., O'Neil, N.J., Trigiante, G., Crook, T., Hsieh, J.K., O'Connor, D.J., Zhong, S., Campargue, I., Tomlinson, M.L., et al. (2003). iASPP oncoprotein is a key inhibitor of p53 conserved from worm to human. Nat. Genet. 33, 162–167.

Bergamaschi, D., Samuels, Y., Sullivan, A., Zvelebil, M., Breyssens, H., Bisso, A., Del Sal, G., Syed, N., Smith, P., Gasco, M., et al. (2006a). iASPP preferentially binds p53 proline-rich region and modulates apoptotic function of codon 72-polymorphic p53. Nat. Genet. *38*, 1133–1141.

Bergamaschi, D., Samuels, Y., Sullivan, A., Zvelebil, M., Breyssens, H., Bisso, A., Del Sal, G., Syed, N., Smith, P., Gasco, M., et al. (2006b). iASPP preferentially binds p53 proline-rich region and modulates apoptotic function of codon 72-polymorphic p53. Nat. Genet. *38*, 1133–1141.

Cheok, C.F., Kua, N., Kaldis, P., and Lane, D.P. (2010). Combination of nutlin-3 and VX-680 selectively targets p53 mutant cells with reversible effects on cells expressing wild-type p53. Cell Death Differ. *17*, 1486–1500.

Chikh, A., Matin, R.N., Senatore, V., Hufbauer, M., Lavery, D., Raimondi, C., Ostano, P., Mello-Grand, M., Ghimenti, C., Bahta, A., et al. (2011). iASPP/p63 autoregulatory feedback loop is required for the homeostasis of stratified epithelia. EMBO J. 30, 4261–4273.

Curtin, J.A., Fridlyand, J., Kageshita, T., Patel, H.N., Busam, K.J., Kutzner, H., Cho, K.H., Aiba, S., Bröcker, E.B., LeBoit, P.E., et al. (2005). Distinct sets of genetic alterations in melanoma. N. Engl. J. Med. 353, 2135–2147.

de Lange, J., Ly, L.V., Lodder, K., Verlaan-de Vries, M., Teunisse, A.F., Jager, M.J., and Jochemsen, A.G. (2012). Synergistic growth inhibition based on small-molecule p53 activation as treatment for intraocular melanoma. Oncogene *31*, 1105–1116.

Emanuel, S., Rugg, C.A., Gruninger, R.H., Lin, R., Fuentes-Pesquera, A., Connolly, P.J., Wetter, S.K., Hollister, B., Kruger, W.W., Napier, C., et al. (2005). The in vitro and in vivo effects of JNJ-7706621: a dual inhibitor of cyclin-dependent kinases and aurora kinases. Cancer Res. 65, 9038–9046

Fogal, V., Hsieh, J.K., Royer, C., Zhong, S., and Lu, X. (2005). Cell cycle-dependent nuclear retention of p53 by E2F1 requires phosphorylation of p53 at Ser315. EMBO J. 24, 2768–2782.

Fredersdorf, S., Milne, A.W., Hall, P.A., and Lu, X. (1996). Characterization of a panel of novel anti-p21Waf1/Cip1 monoclonal antibodies and immunochemical analysis of p21Waf1/Cip1 expression in normal human tissues. Am. J. Pathol. *148*, 825–835.

Gembarska, A., Luciani, F., Fedele, C., Russell, E.A., Dewaele, M., Villar, S., Zwolinska, A., Haupt, S., de Lange, J., Yip, D., et al. (2012). MDM4 is a key therapeutic target in cutaneous melanoma. Nat. Med. *18*, 1239–1247.

Georgieva, J., Sinha, P., and Schadendorf, D. (2001). Expression of cyclins and cyclin dependent kinases in human benign and malignant melanocytic lesions. J. Clin. Pathol. *54*, 229–235.

Houben, R., Hesbacher, S., Schmid, C.P., Kauczok, C.S., Flohr, U., Haferkamp, S., Müller, C.S., Schrama, D., Wischhusen, J., and Becker, J.C. (2011). High-level expression of wild-type p53 in melanoma cells is frequently associated with inactivity in p53 reporter gene assays. PLoS ONE 6, e22096.

Ji, Z., Njauw, C.N., Taylor, M., Neel, V., Flaherty, K.T., and Tsao, H. (2012). p53 rescue through HDM2 antagonism suppresses melanoma growth and potentiates MEK inhibition. J. Invest. Dermatol. *132*, 356–364.

Jiang, L., Siu, M.K., Wong, O.G., Tam, K.F., Lu, X., Lam, E.W., Ngan, H.Y., Le, X.F., Wong, E.S., Monteiro, L.J., et al. (2011). iASPP and chemoresistance in ovarian cancers: effects on paclitaxel-mediated mitotic catastrophe. Clin. Cancer Res. 17, 6924–6933.

Johnson, L.N. (2011). Substrates of mitotic kinases. Sci. Signal. 4, pe31.

Joseph, E.W., Pratilas, C.A., Poulikakos, P.I., Tadi, M., Wang, W., Taylor, B.S., Halilovic, E., Persaud, Y., Xing, F., Viale, A., et al. (2010). The RAF inhibitor PLX4032 inhibits ERK signaling and tumor cell proliferation in a V600E BRAF-selective manner. Proc. Natl. Acad. Sci. USA 107, 14903–14908.

Muthusamy, V., Hobbs, C., Nogueira, C., Cordon-Cardo, C., McKee, P.H., Chin, L., and Bosenberg, M.W. (2006). Amplification of CDK4 and MDM2 in malignant melanoma. Genes Chromosomes Cancer 45, 447–454.

Notari, M., Hu, Y., Koch, S., Lu, M., Ratnayaka, I., Zhong, S., Baer, C., Pagotto, A., Goldin, R., Salter, V., et al. (2011). Inhibitor of apoptosis-stimulating protein of p53 (iASPP) prevents senescence and is required for epithelial stratification. Proc. Natl. Acad. Sci. USA *108*, 16645–16650.

Olsen, J.V., Vermeulen, M., Santamaria, A., Kumar, C., Miller, M.L., Jensen, L.J., Gnad, F., Cox, J., Jensen, T.S., Nigg, E.A., et al. (2010). Quantitative phosphoproteomics reveals widespread full phosphorylation site occupancy during mitosis. Sci. Signal. *3*, ra3.

Polsky, D., Bastian, B.C., Hazan, C., Melzer, K., Pack, J., Houghton, A., Busam, K., Cordon-Cardo, C., and Osman, I. (2001). HDM2 protein overexpression, but not gene amplification, is related to tumorigenesis of cutaneous melanoma. Cancer Res. *61*, 7642–7646.

Poulikakos, P.I., and Solit, D.B. (2011). Resistance to MEK inhibitors: should we co-target upstream? Sci. Signal. 4, pe16.

Robinson, R.A., Lu, X., Jones, E.Y., and Siebold, C. (2008). Biochemical and structural studies of ASPP proteins reveal differential binding to p53, p63, and p73. Structure 16, 259–268.

Rudolf, E., Rudolf, K., and Cervinka, M. (2011). Camptothecin induces p53-dependent and -independent apoptogenic signaling in melanoma cells. Apoptosis *16*, 1165–1176.

Sachdev, S., Hoffmann, A., and Hannink, M. (1998). Nuclear localization of IkappaB alpha is mediated by the second ankyrin repeat: the IkappaB alpha ankyrin repeats define a novel class of cis-acting nuclear import sequences. Mol. Cell. Biol. 18, 2524–2534.

Samuels-Lev, Y., O'Connor, D.J., Bergamaschi, D., Trigiante, G., Hsieh, J.K., Zhong, S., Campargue, I., Naumovski, L., Crook, T., and Lu, X. (2001). ASPP proteins specifically stimulate the apoptotic function of p53. Mol. Cell 8, 781–794.

Slee, E.A., Gillotin, S., Bergamaschi, D., Royer, C., Llanos, S., Ali, S., Jin, B., Trigiante, G., and Lu, X. (2004). The N-terminus of a novel isoform of human iASPP is required for its cytoplasmic localization. Oncogene *23*, 9007–9016.

Slee, E.A., Benassi, B., Goldin, R., Zhong, S., Ratnayaka, I., Blandino, G., and Lu, X. (2010). Phosphorylation of Ser312 contributes to tumor suppression by p53 in vivo. Proc. Natl. Acad. Sci. USA 107, 19479–19484.

Song, Y., Zhao, C., Dong, L., Fu, M., Xue, L., Huang, Z., Tong, T., Zhou, Z., Chen, A., Yang, Z., et al. (2008). Overexpression of cyclin B1 in human esophageal squamous cell carcinoma cells induces tumor cell invasive growth and metastasis. Carcinogenesis 29, 307–315.

Terzian, T., Torchia, E.C., Dai, D., Robinson, S.E., Murao, K., Stiegmann, R.A., Gonzalez, V., Boyle, G.M., Powell, M.B., Pollock, P.M., et al. (2010). p53

Cancer Cell

Restoring p53 Function in Melanoma



prevents progression of nevi to melanoma predominantly through cell cycle regulation. Pigment Cell Melanoma Res. 23, 781-794.

Tseng, H.Y., Jiang, C.C., Croft, A., Tay, K.H., Thorne, R.F., Yang, F., Liu, H., Hersey, P., and Zhang, X.D. (2010). Contrasting effects of nutlin-3 on TRAILand docetaxel-induced apoptosis due to upregulation of TRAIL-R2 and Mcl-1 in human melanoma cells. Mol. Cancer Ther. 9, 3363-3374.

Van Impe, K., Hubert, T., De Corte, V., Vanloo, B., Boucherie, C., Vandekerckhove, J., and Gettemans, J. (2008). A new role for nuclear transport factor 2 and Ran: nuclear import of CapG. Traffic 9, 695-707.

Vu, B.T., and Vassilev, L. (2011). Small-molecule inhibitors of the p53-MDM2 interaction. Curr. Top. Microbiol. Immunol. 348, 151-172.

Wang, Y., and Prives, C. (1995). Increased and altered DNA binding of human p53 by S and G2/M but not G1 cyclin-dependent kinases. Nature 376, 88-91.

Yang, J.P., Hori, M., Sanda, T., and Okamoto, T. (1999). Identification of a novel inhibitor of nuclear factor-kappaB, RelA-associated inhibitor. J. Biol. Chem. 274, 15662-15670.

Yang, G., Rajadurai, A., and Tsao, H. (2005). Recurrent patterns of dual RB and p53 pathway inactivation in melanoma. J. Invest. Dermatol. 125, 1242-

Zhang, Y., Xiong, Y., and Yarbrough, W.G. (1998). ARF promotes MDM2 degradation and stabilizes p53: ARF-INK4a locus deletion impairs both the Rb and p53 tumor suppression pathways. Cell 92, 725-734.